Optimized pulses for Raman excitation through the continuum: Verification using the multiconfigurational time-dependent Hartree-Fock method

Loren Greenman,[1,2,*] K. Birgitta Whaley,[2,1] Daniel J. Haxton,[1] and C. William McCurdy[1,3]

[1]*Chemical Sciences Division, Lawrence Berkeley National Laboratory, Berkeley, California 94720, USA*

[2]*Department of Chemistry and Kenneth S. Pitzer Center for Theoretical Chemistry, University of California, Berkeley, California 94720, USA*

[3]*Department of Chemistry, University of California, Davis, California 95616, USA*

(Received 29 December 2016; published 13 July 2017)

We have verified a mechanism for Raman excitation of atoms through continuum levels previously obtained by quantum optimal control using the multiconfigurational time-dependent Hartree-Fock (MCTDHF) method. For the optimal control, which requires running multiple propagations to determine the optimal pulse sequence, we used the computationally inexpensive time-dependent configuration interaction singles (TDCIS) method. TDCIS captures all of the necessary correlation of the desired processes but assumes that ionization pathways reached via double excitations are not present. MCTDHF includes these pathways and all multiparticle correlations in a set of time-dependent orbitals. The mechanism that was determined to be optimal in the Raman excitation of the Ne $1s^2 2s^2 2p^5 3p^1$ valence state via the metastable $1s^2 2s^1 2p^6 3p^1$ resonance state involves a sequential resonance-valence excitation. First, a long pump pulse excites the core-hole state, and then a shorter Stokes pulse transfers the population to the valence state. This process represents the first step in a multidimensional x-ray spectroscopy scheme that will provide a local probe of valence electronic correlations. Although at the optimal pulse intensities at the TDCIS level of theory the MCTDHF method predicts multiple ionization or excitation ionization of the atom, at slightly lower intensities (reduced by a factor of about 4) the TDCIS mechanism is shown to hold qualitatively. Quantitatively, the MCTDHF populations are reduced from the TDCIS calculations by a factor of 4.

DOI: 10.1103/PhysRevA.96.013411

I. INTRODUCTION

Whereas linear spectroscopy directly measures the energies of states via the first-order response function, multidimensional spectroscopy measures couplings between states using higher-order response functions. Multidimensional spectroscopies are currently used to measure couplings in the regimes of radio waves (nuclear magnetic resonance) [1–3], infrared (vibrational) [4,5], and ultraviolet-visible (UV-vis) (photon echo) [6–10]. An x-ray analog of such spectroscopies could be used to measure couplings between localized core-hole excitations [11,12]. Such couplings are due to valence electron interactions, and therefore x-ray multidimensional spectroscopy provides a local probe of valence excitations. However, complications arise due to the high energy of x-ray pulses, which can ionize samples or cause other unwanted processes to occur.

Multidimensional spectroscopy uses two or more frequencies to measure the coupling between two excited states of an atom or molecule. In multidimensional x-ray techniques, localized core-hole states can be addressed by one or more of these frequencies. An x-ray Raman excitation of a valence excited state in a molecule can be correlated with another core-hole excitation located far away to measure spatial energy transfer [11]. Two Raman excitations can be used with a variable time delay to probe the relaxation of valence excitons [13]. In some schemes, the phases between the different states are used to measure the coherence between two excited states or to enhance the signal considerably. It is therefore important to ensure that the high energy of the x rays does not ionize the system or initiate spectator processes that reduce the coherence.

Two of us have recently obtained optimized pulses in a theoretical study that perform the first crucial step of a multidimensional x-ray scheme while avoiding ionization [14]. The design of the pulses in that study was accomplished by combining Krotov's optimal control method [15–20] with time-dependent configuration interaction singles (TDCIS) electronic dynamics including the ionization continuum [21,22]. The TDCIS method is a good choice for optimal control calculations; it is computationally cheap and captures low-order electron correlation by including all singly excited electronic configurations. However, TDCIS ignores multiply excited pathways, and so the reliability of the optimal pulses in an experimental setting is unclear. These multiply excited pathways could lead to ionization, reducing the overall yield of the final result. They could also reduce the coherence predicted by TDCIS by interacting with the singly excited pathway and altering the phases of the states. In this work, we use the multiconfigurational time-dependent Hartree-Fock (MCTDHF) [23,24] method to verify that the pulses that were optimized using TDCIS to accomplish the population transfer shown in Fig. 1 in the Ne atom perform similar population transfers when the electronic dynamics are described with the inclusion of higher-order electron correlation. MCTDHF includes all excitation pathways within a subset of orbitals, which are time dependent (unlike TDCIS, which uses time-independent orbitals).

This method simultaneously describes stable valence states, autoionizing states, and the photoionization continua, which are involved in these experiments, and this approach has been previously explored and developed by several groups [25–32]. Briefly, our implementation solves the time-dependent Schrödinger equation in full dimensionality, with all electrons active. It rigorously treats the ionization continua for both single and multiple ionization using complex exterior scaling.

*lgreenman@lbl.gov

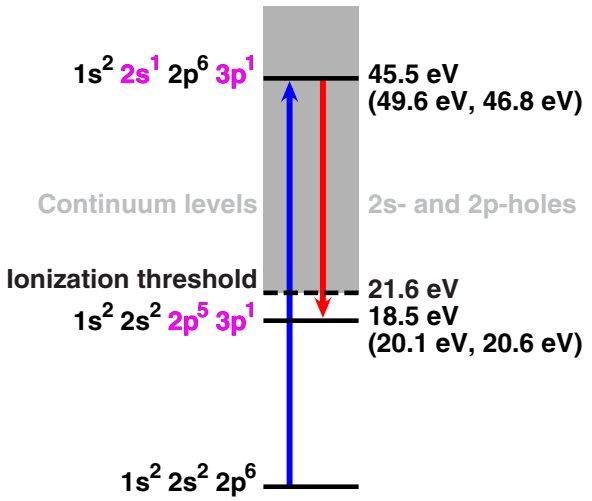

FIG. 1. The target Raman process is pictured. The pump (blue, left) pulse excites the intermediate ($2s$-$3p$) state, then the Stokes (red, right) pulse transfers the population to the desired ($2p$-$3p$) state. The experimental energy levels are given, along with the TDCIS (from diagonalization) and MCTDHF (determined as in Fig. 4) energy levels in parentheses.

As more orbitals, and larger grids for describing them, are included, the MCTDHF wave function formally converges to the exact many-electron solution, but here the limits of computational practicality were reached with the inclusion of full configuration interaction with nine time-dependent orbitals. While it is possible to do larger calculations on Ne using MCTDHF [33] (we have used up to 14 orbitals), we determined that these calculations required much smaller time steps to accurately determine the (small) populations of the states involved in the Raman process. Nonetheless, these calculations provide a substantial test of the assumptions of the simpler and more computationally tractable TDCIS approach.

Previously, we used MCTDHF to perform Raman excitation of atomic lithium [34] and the NO molecule [35]. In both of those studies, as in Ref. [14] and also in the current work, the first step in a multidimensional scheme (such as those described above) is attempted, and the intermediate state of the Raman process is a resonance state above the level of the electronic ionization continuum. Additionally, all of these investigations have found adiabatic mechanisms such as stimulated Raman adiabatic passage (STIRAP) [36] to be ineffective at the energy and time scales of interest. In our previous MCTDHF studies [34,35], the potentially large amount of background ionization due to absorption of the x-ray pulses by spectator orbitals was avoided by choosing inner core levels to address with the pulses. The high-energy x rays that address these levels have a much lower cross section for absorption by spectator orbitals. In the case of of our previous study of Raman population transfer in the Li atom [34], there were no occupied p orbitals to contribute to background ionization. In contrast, the previous study for neon [14] employed optimal control theory to find pulses that minimize background ionization but penalizes distance from some guess pulse. A mechanism was thereby found to excite a Raman excitation using pulses with lower energies, although a smaller fraction of the final wave function is in the Raman state. That study also considered coherent excitation of the Raman state [14], and optimal pulses were also obtained that excite the Raman state with a fixed phase relative to the ground state.

These optimizations performed with TDCIS produced specific pulses but also revealed a more general mechanism for generating pulse sequences that perform x-ray Raman while avoiding ionization [14]. In this sequential mechanism, a long pump pulse is first used to selectively excite population from the ground state to the intermediate state, and then a shorter Stokes pulse is used to transfer population from the intermediate state to the desired state. The long pump pulse selects the transition to the intermediate state, which is located close in energy to a dense number of continuum states, and avoids background transitions to those states. If a specific phase is desired between the Raman state and ground state, it can be imprinted via the carrier-envelope phase of the pump pulse [14]. The length of the Stokes pulse is somewhat flexible, but it must be short enough to overcome autoionization from the intermediate state. The ideal placement of the Stokes pulse is near the peak of the intermediate-state population, which TDCIS predicts to be slightly before the pump pulse maximum for a pump pulse on the order of 50 fs.

Here, as before [14], we use Ne as an example because of its accessibility to tabletop experiments through the rapidly advancing availability of XUV high harmonic generation and free-electron lasers such as FERMI@Elettra [37]. The levels we are targeting are shown in Fig. 1. The intermediate state is the $2s$-$3p$ state of Ne, which lies above the ionization threshold. The target state is the $2p$-$3p$ valence excitation.

We find that up to a factor less than an order of magnitude, electron correlation effects captured using MCTDHF do not destroy the efficacy of the optimal pulses. However, this is true only up to a certain intensity, above which multiple-ionization and excitation-ionization pathways make TDCIS unreliable.

II. THEORY

Both the time-dependent configuration interaction singles (TDCIS) [21,22] method and the multiconfigurational time-dependent Hartree-Fock (MCTDHF) [23,24] method choose a reference configuration ($|\Phi_0\rangle$) that is an antisymmetrized product of N_e single-particle orbitals,

$$|\Phi_0\rangle = |\phi_1\phi_2\ldots\phi_{N_e}\rangle. \tag{1}$$

Both methods describe the many-electron wave function using this reference and configurations obtained by exciting particles from the reference,

$$\left|\Phi_i^a\right\rangle = \hat{a}_a^\dagger \hat{a}_i|\Phi_0\rangle, \tag{2}$$

$$\left|\Phi_{i,j}^{a,b}\right\rangle = \hat{a}_a^\dagger \hat{a}_b^\dagger \hat{a}_j \hat{a}_i|\Phi_0\rangle, \ldots, \tag{3}$$

where i,j denote orbitals occupied in the reference, a,b denote unoccupied orbitals, and $\hat{a}$ and $\hat{a}^\dagger$ denote annihilation and creation operators, respectively.

In the configuration interaction singles (CIS) method, the reference [Eq. (1)] and *all* singly excited configurations [Eq. (2)] are included (up to a very high-energy cutoff),

$$|\Psi(t)\rangle = \alpha_0(t)|\Phi_0\rangle + \sum_{i,a}\alpha_i^a(t)\left|\Phi_i^a\right\rangle. \tag{4}$$

In this configuration space, dynamic electron correlation between singly excited configurations is taken into account. Due to Brillouin's theorem, there is no mixing between the reference configuration and excited configurations due to Coulomb interactions. CIS therefore provides a first-order description of excited states dominated by single-particle configurations. Excitations that involve multiple occupied orbitals cannot be described by CIS. Time-dependent CIS (TDCIS) uses time-dependent coefficients on the CIS configurations to describe the time-evolving wave function. The orbitals ϕ_i remain time *independent*, in contrast to the MCTDHF method. TDCIS cannot describe multiple-ionization or excitation-ionization pathways.

The MCTDHF method [23–28,38], as implemented in Refs. [23,24], uses a smaller subset of N_o orbitals, $\{\phi_{\rm sub}\} = \{\phi_1, \ldots, \phi_{N_o}\}$, but includes all configurations in this subset. This means that multiply ionized pathways can now be described. The coefficients on each configuration and the shape of the orbitals that define the reference and excited configurations are both time dependent,

$$|\Psi(t)\rangle = \alpha_0(t)|\Phi_0(t)\rangle + \sum_{i,a\in\{\phi_{\rm sub}\}} \alpha_i^a(t)\left|\Phi_i^a(t)\right\rangle + \sum_{i,j,a,b\in\{\phi_{\rm sub}\}} \alpha_{i,j}^{a,b}(t)\left|\Phi_{i,j}^{a,b}(t)\right\rangle + \cdots \qquad (5)$$

It should be noted that an implementation using finite-element discrete variable representation (DVR) grids of MCTDHF using restricted configuration spaces has also been developed [39]. MCTDHF in a small (practical) space of orbitals mainly captures static (nondynamic) correlation, i.e., the contribution from configurations that at zeroth order define the wave function. For instance, double ionization from the core is described at zeroth order using a doubly excited configuration; TDCIS cannot describe this. While reducing the number of orbitals leads to a greater amount of dynamic correlation being left out, the time-dependent nature of the orbitals could possibly reintroduce some dynamic correlation back into the calculation. Furthermore, dynamic correlation tends to lead only to quantitative, and not qualitative, corrections to the wave function.

One further difference between the implementation of the TDCIS method used in Ref. [14] and the implementation of the MCTDHF method used here is the description of the ionization continuum. The TDCIS implementation uses a complex absorbing potential (CAP) [21,40,41], an imaginary quadratic potential that is turned on after a cutoff radius. CAPs can be tuned to capture a small number of resonance energies correctly, but they can also perturb the bound states and continuum states outside of the region for which they are tuned. The MCTDHF implementation instead uses exterior complex scaling (ECS) [42,43], in which the spatial coordinates are scaled into the complex plane by an angle θ. Grid implementations of ECS have been shown to effectively treat single- and double-ionization continua [43], and they do not perturb the bound states. It should be noted that either ECS or a CAP can be used in both TDCIS and MCTDHF; the difference here lies in these specific implementations.

Comparing MCTDHF and TDCIS propagations using the optimal pulses previously determined with Krotov's method [14] thus provides a fuller view of the time-dependent processes in the x-ray Raman excitation of atoms.

The MCTDHF calculations presented here were obtained using a space of nine time-dependent spatial orbitals: the $1s$, $2s$, $2p$, $3s$, and $3p$ orbitals of Ne. There are 4116 configuration-state functions in this active space. The orbitals are described with a finite-element version of the discrete variable representation (DVR) in the radial degree of freedom, a DVR in the polar angle, θ, and analytical functions of the azimuthal angle, $\exp(im\varphi)$. We used a radial grid of six 9.0 Bohr elements, each with 19 grid points, an angular grid of fifth order in θ, and analytic functions capable of describing angular momentum states of up to $m = 2$. The last element was complex scaled using an angle of 0.4 radians.

III. RESULTS AND DISCUSSION

The mechanism for x-ray Raman excitation of atoms while avoiding ionization is as follows: first, a long pump pulse is used to selectively excite the intermediate state (the $2s$-$3p$ state of Ne), followed by a shorter Stokes pulse that beats the autoionization of the intermediate state and transfers the population to the desired state (in Ne, the $2p$-$3p$ state). This mechanism was discovered in Ref. [14] using TDCIS and optimal control theory, and it was used there to develop experimentally realizable pulses. A 50 fs, 71 μJ pump pulse and 0.5 fs, 0.71 μJ Stokes pulse represent one choice of pulses. Other options were presented in Ref. [14] using variable lengths of the Stokes pulse. The peak intensity of the pump pulse was 6.1×10^{14} W/cm^2.

Since MCTDHF and TDCIS have different descriptions of the electron correlation, the transition frequencies at each level of theory will be different. Therefore, the MCTDHF transition frequencies must first be obtained. We accomplished this by running various continuous-wave (cw) pulses with many central frequencies. The relevant MCTDHF frequencies can also be determined by Fourier transforming the dipole after exciting with a short pulse, but this requires long propagations after the pulse and it is also difficult to get some resonance states in this manner.

Figure 2 shows the results of one such set of computations with the peak intensities from the TDCIS optimal pulses. The intermediate-state populations are shown, with colors ranging from red to blue for central frequencies from 46.8 to 48.0 eV. The optimal TDCIS intermediate-state populations reached around 0.08, but the MCTDHF populations in Fig. 2 are much lower, i.e., less than 0.01. At these intensities, the MCTDHF and TDCIS results differ significantly and the most likely explanation is that multiply ionized pathways are important at these intensities. While the effects of multiparticle correlations present in MCTDHF cannot be ruled out as the cause of the difference, we note that Fig. 2 shows very fast intermediate-state population depletion ($\sim$2 fs), which suggests ionization from this state. This ionization may result in a multiply ionized atom or in an atom that has been ionized from an excited state, resulting, for instance, in a $1s^2 2s^1 2p^5 3s^1$ + continuum electron state. TDCIS does not take ionization pathways such as these into account.

In Fig. 3, the TDCIS response to cw pulses with the same and higher intensities is shown. While the MCTDHF

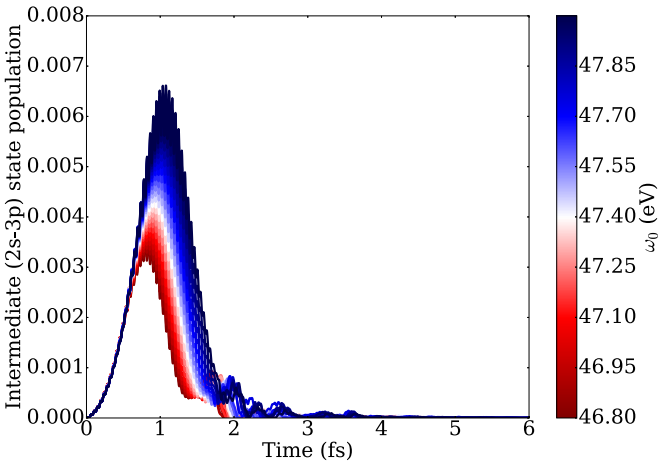

FIG. 2. MCTDHF intermediate-state ($2s$-$3p$) populations for cw pulses at intensities optimized using TDCIS. Pulses are shown for a number of different central frequencies ω_0 [see color bar: small ω_0 in red (lighter) shades and at lower populations, larger ω_0 in blue (darker) shades and at higher populations]. The opening of double- and higher-ionization and excitation-ionization channels imposes an intensity limit on the pulses. The optimal intensity at the TDCIS level of theory is above this limit, which leads to ionization rather than populating the intermediate state.

intermediate-state population depletes at 2 fs, TDCIS predicts stable populations at much longer time scales at an intensity of 6.1×10^{14} W/cm^2. Even at higher intensities, TDCIS predicts Ne $2s$-hole populations greater than 0.02 and no depletion of this population. At an intensity of 6×10^{14} W/cm^2, approximately 3.5 photons/fs cross the atomic radius of Ne, which could lead to the absorption of two or more photons and ionize

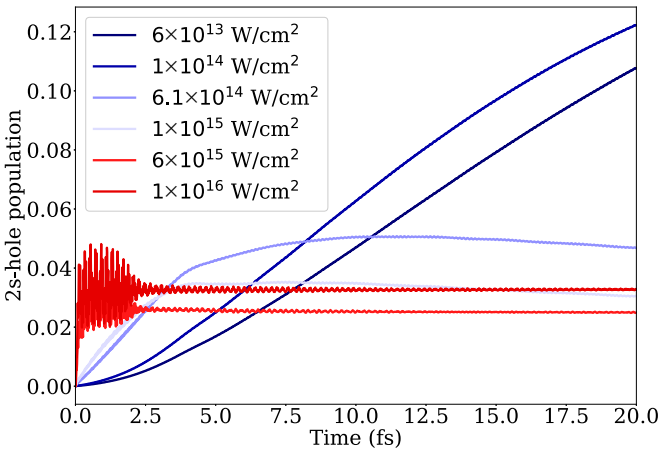

FIG. 3. TDCIS $2s$-hole population for cw pulses at a number of different intensities. These correlate with the intermediate-state ($2s$-$3p$) populations. Higher intensities [red (light gray)] oscillate and reach maximum populations between 2–4% and lower intensities [blue (darker gray)] rise to much higher populations near 10%. While for MCTDHF at the optimal intensity of 6.1×10^{14} W/cm^2 (Fig. 2) the population is depleted at 2 fs, at the TDCIS level of theory populations are stable even at much higher intensities. Since this quick population depletion is dependent on the pulse intensity and is not seen at lower intensities, it is more likely due to ionization pathways rather than the additional correlation present in MCTDHF.

the atom. A reduction of the intensity by a factor of about 4, however, returns the system to the single-excitation regime, which TDCIS describes well.

In Fig. 4, the lower-intensity regimes are shown. Intermediate-state populations for peak intensities of 10^{14}, 1 and 5×10^{13}, and 5×10^{12} W/cm^2 are shown. At these intensities, the intermediate state is populated at the same order of magnitude as estimated by TDCIS at the same intensities. The population revivals seen in Fig. 4 are further evidence that multiparticle ionization pathways are the cause of the discrepancies between TDCIS and MCTDHF seen at higher intensities. The dependence of the population depletion calculated by MCTDHF on the intensity is not seen in TDCIS (Fig. 3), but at intensities slightly lower than 6.1×10^{14} W/cm^2, TDCIS and MCTDHF qualitatively agree. As expected from TDCIS, the higher intensities populate the intermediate state more (as long as the multi-ionization threshold is avoided). At 10^{14} and 5×10^{13} W/cm^2, intermediate-state populations of about 0.02 are reached. This is a factor of 4 lower than the TDCIS result. For both of these intensities, the optimal pump-pulse central frequency is found to be 46.8 eV. At the lower intensities, the intermediate state is not populated very much. This is also found at the TDCIS level of theory. As the intensity of the pump pulse is lowered, the optimal central frequency is redshifted.

With the peak intensity and central frequency for the pump pulse fixed at the values determined using the cw pulses, we test the effect of increasing the duration π/Ω of pulses shaped using a $\sin^2(\Omega t)$ function. The results are shown in Fig. 5. Similar to what was seen in the TDCIS results [14], increasing the pump-pulse length is found to be generally favorable. The maximum intermediate-state population increases largely at first, and then slightly as the pulse is made longer. An intermediate-state population of about 0.03 can be reached using a 50 fs pump pulse, but at these pulse durations it again appears that ionization pathways start to interfere. For the 30, 40, and 50 fs pulse durations, a dip in the population can be seen that suggests that higher-order effects are beginning to occur. Since the maximum intermediate-state population increases only slightly above 20 fs and there are no observable multiparticle ionization effects at this pulse duration, we use the 20 fs pump pulse when determining the optimal Stokes pulse parameters at the MCTDHF level.

Using the same method of determining the optimal central frequency and peak intensity of the Stokes pulse with cw pulses, we determined that the intensity of the Stokes pulse predicted by TDCIS does not introduce additional ionization pathways. Additionally, a number of calculations were run to determine the optimal central time of the Stokes pulse. The resulting set of pump and Stokes pulses was used to determine the populations of the intermediate $2s$-$3p$ and desired $2p$-$3p$ states for Raman excitation of Ne and compared with the optimal TDCIS pulse set in Fig. 6.

Qualitatively, the pulses obtained with TDCIS and control theory are similar to those obtained with MCTDHF and some parameter optimization. MCTDHF is expensive and therefore ill suited to control theory calculations, which require multiple forward and backward propagations with different laser pulses. However, we have shown here that TDCIS is adequate for control calculations, provided that an intensity threshold is avoided. This threshold is most likely that of multiparticle

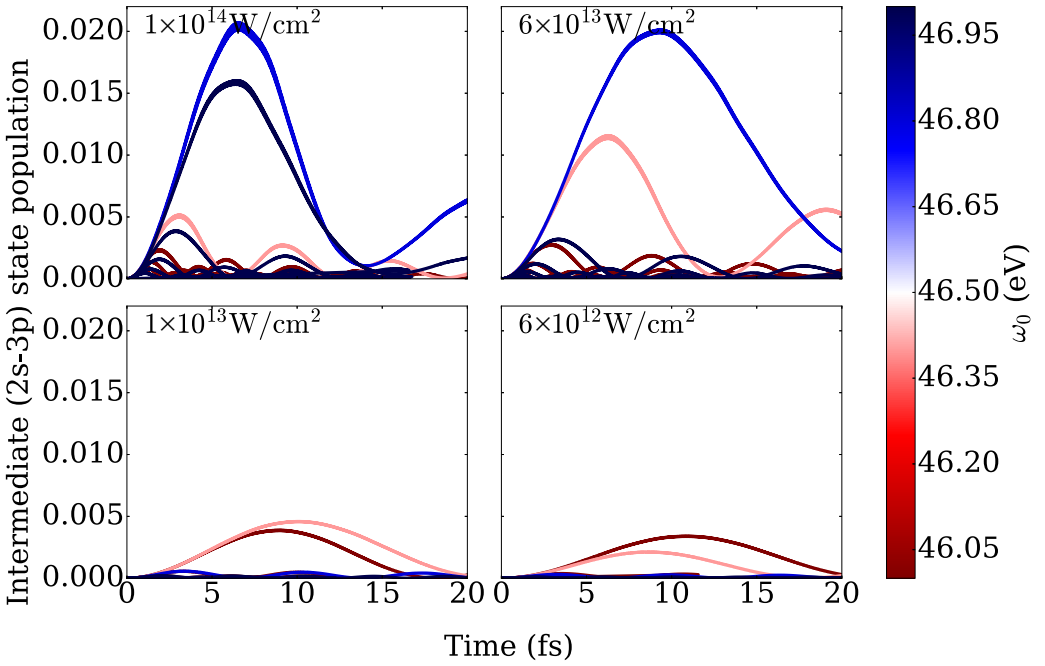

FIG. 4. Intermediate-state ($2s$-$3p$) populations are shown at the MCTDHF level of theory for intensities lower than the optimal TDCIS intensity. As in Fig. 2, higher central frequencies appear in blue (dark gray) and lower frequencies in red (lighter gray). The multiparticle ionization channels are now closed and the orders of magnitude of the TDCIS and MCTDHF intermediate-state populations are now the same. The optimal central frequency for intermediate-state population redshifts as the intensity is lowered. At an intensity of 1×10^{14} W/cm^2, the optimal central frequency of the pump pulse is 46.8 eV.

ionizations due to the intensity-dependent behavior of the population depletion point. It is easy to enforce such a threshold in optimal control calculations by imposing a penalty on the maximum intensity of the pulse.

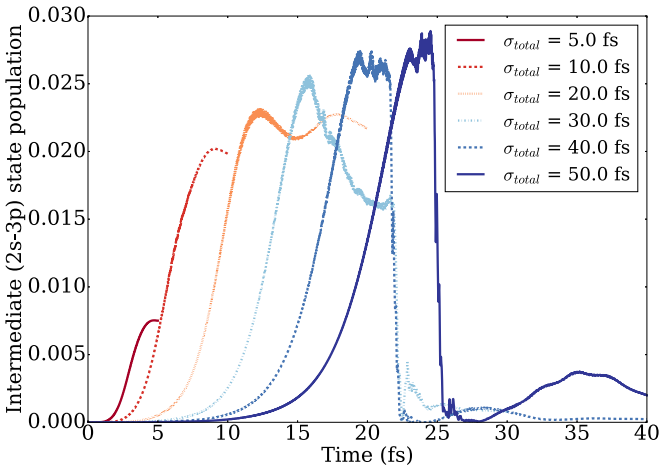

FIG. 5. The intermediate-state ($2s$-$3p$) population during the pulse is shown for increasing pulse lengths σ_{total}, where the pulse envelope is given by $\mathcal{E}(t) = \mathcal{E}_0 \sin^2(\Omega t)$ and $\sigma_{\text{total}} = \pi/\Omega$. The maximum intermediate-state population increases with pulse length, with the increases slowing as the pulse length grows at an intensity of 10^{14} W/cm^2. The TDCIS optimal strategy is to maximize the intermediate-state population and then use the Stokes pulse to transfer the intermediate-state population to the desired state, and the maximum intermediate-state population reachable is around 0.03. Longer pump pulses seem also to induce ionization around the peak of the pulse.

The optimal pulse sequence represents a simple sequential population of the intermediate state followed by population transfer to the desired state. At the TDCIS level of theory, the intermediate state is populated to a level of 0.08, and about half of this population can be transferred to the desired state. We found in Ref. [14] that coupling between excitation channels induced by electron correlation keeps the entire population of the intermediate state from being transferred to the desired

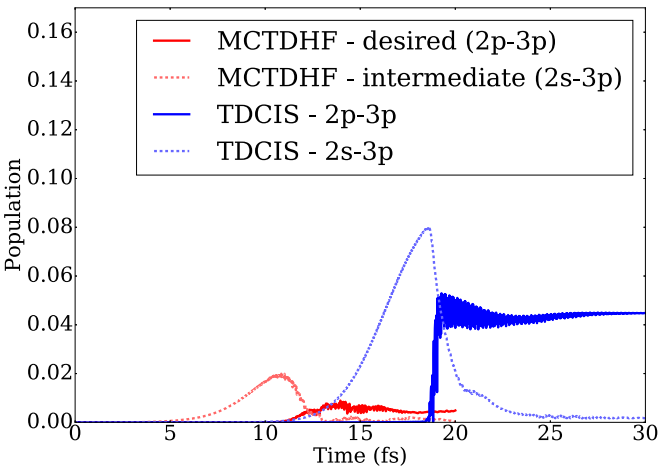

FIG. 6. The optimal TDCIS pulse [populations in blue (darker gray)] is compared with a similar (shorter) MCTDHF pulse [populations in red (lighter gray) and at lower populations] with the same time ordering. The desired state (dark lines) and intermediate states (light lines) are shown. The qualitative features of the TDCIS and MCTDHF results are the same. The MCTDHF populations are smaller by a factor of about 4.

state. At the MCTDHF level of theory, we have already determined that the intermediate state can be populated to a level of 0.02 and this can again be seen in Fig. 6.

IV. CONCLUSION

We have used the multiconfigurational time-dependent Hartree-Fock (MCTDHF) method to verify the performance of optimal pulses for x-ray Raman excitation of atoms. This excitation represents the first step towards multidimensional x-ray spectroscopy, a tool for the direct and local measurement of electronic interactions in valence levels. The pulses were previously obtained in Ref. [14] using quantum optimal control theory combined with the time-dependent configuration interaction singles (TDCIS) method. MCTDHF includes multiple-excitation and excitation-ionization pathways that TDCIS does not, and these were found likely to impose an important intensity constraint on the optimal control calculations. Below these intensities, however, the qualitative features of the processes predicted by TDCIS were nevertheless found to extend to the more detailed calculations. TDCIS, therefore, is an appropriate tool for optimal control calculations, having the advantages of speed while not sacrificing qualitative accuracy. In systems where strong correlation is present, however, modifications to TDCIS are likely to be necessary for qualitative accuracy.

Using the combined Krotov optimal control and TDCIS method, we had previously determined a mechanism for avoiding ionization while performing the x-ray Raman excitation of atoms [14]. First, the intermediate state is excited using a long pump pulse to selectively address the frequency of the desired transition. Then, a short Stokes pulse is applied near the maximum intermediate-state population to drive population to the desired valence state. This pulse sequence avoids ionization, which is mainly due to direct ionization of the spectator orbitals (the $2p$ orbitals in the case of Ne). This general scheme is supported by the MCTDHF calculations; however, some details of its implementation differ from TDCIS. At the intensities that are found to be optimal using TDCIS, multiparticle ionization pathways are found to occur using MCTDHF. These processes dominate and very little population can be transferred to the intermediate state. At slightly lower intensities, the mechanism found using TDCIS is again qualitatively successful. Quantitatively, a factor of about 4 differentiates the TDCIS and MCTDHF populations. This factor is likely due to the competing multiply excited pathways that are not present in TDCIS.

Using TDCIS, we determined that x-ray Raman excitation of Ne was experimentally feasible at the free-electron laser facility FERMI@Elettra [37]. The pulses we have now found to be successful at the MCTDHF level of theory are also possible at that facility. Specifically, a pump pulse with a duration of 20 fs and power of 0.6 μJ (assuming a spot size diameter of 10 μm) can be used to Raman excite Ne and avoid ionization.

ACKNOWLEDGMENTS

Work performed at Lawrence Berkeley National Laboratory was supported by the U.S. Department of Energy Office of Basic Energy Sciences, Division of Chemical Sciences Contract No. DE-AC02-05CH11231 and made use of the resources of the National Energy Research Scientific Computing Center, a U.S. Department of Energy Office of Science User Facility. K.B.W. was supported through the Scientific Discovery through Advanced Computing (SciDAC) program funded by the U.S. Department of Energy, Office of Science, Advanced Scientific Computing Research, and Basic Energy Sciences. We also acknowledge funding through the U.S. Department of Energy Early Career program and the Peder Sather Center.

[1] R. R. Ernst, G. Bodenhausen, A. Wokaun *et al.*, *Principles of Nuclear Magnetic Resonance in One and Two Dimensions*, Vol. 14 (Clarendon Press, Oxford, 1987).
[2] M. Sattler, J. Schleucher, and C. Griesinger, Prog. Nucl. Magn. Reson. Spectrosc. **34**, 93 (1999).
[3] V. Kanelis, J. D. Forman-Kay, and L. E. Kay, IUBMB Life **52**, 291 (2001).
[4] D. S. Larsen, K. Ohta, Q.-H. Xu, M. Cyrier, and G. R. Fleming, J. Chem. Phys. **114**, 8008 (2001).
[5] M. Khalil, N. Demirdöven, and A. Tokmakoff, J. Phys. Chem. A **107**, 5258 (2003).
[6] S. Mukamel, Annu. Rev. Phys. Chem. **51**, 691 (2000).
[7] D. M. Jonas, Annu. Rev. Phys. Chem. **54**, 425 (2003).
[8] G. S. Engel, T. R. Calhoun, E. L. Read, T.-K. Ahn, T. Manl, Y.-C. Cheng, R. E. Blankenship, and G. R. Fleming, Nature (London) **446**, 782 (2007).
[9] J. D. Biggs, Y. Zhang, D. Healion, and S. Mukamel, J. Chem. Phys. **136**, 174117 (2012).
[10] S. Mukamel, D. Healion, Y. Zhang, and J. D. Biggs, Annu. Rev. Phys. Chem. **64**, 101 (2013).
[11] S. Tanaka and S. Mukamel, Phys. Rev. Lett. **89**, 043001 (2002).
[12] S. Mukamel, D. Abramavicius, L. Yang, W. Zhuang, I. V. Schweigert, and D. V. Voronine, Acc. Chem. Res. **42**, 553 (2009).
[13] Y. Zhang, W. Hua, K. Bennett, and S. Mukamel, in *Density-Functional Methods for Excited States*, edited by N. Ferré, M. Filatov, and M. Huix-Rotllant (Springer, Switzerland, 2014), pp. 273–345.
[14] L. Greenman, C. P. Koch, and K. B. Whaley, Phys. Rev. A **92**, 013407 (2015).
[15] D. Tannor, V. Kazakov, and V. Orlov, in *Time-dependent Quantum Molecular Dynamics*, edited by J. Broeckhove and L. Lathouwers (Plenum, New York, 1992), pp. 347–360.
[16] J. Somlói, Vladimir A. Kazakov, and D. J. Tannor, Chem. Phys. **172**, 85 (1993).
[17] A. I. Konnov and V. F. Krotov, Autom. Remote Control (Engl. Transl.) **60**, 1427 (1999).
[18] A. Bartana, R. Kosloff, and D. J. Tannor, Chem. Phys. **267**, 195 (2001).

[19] J. P. Palao, R. Kosloff, and C. P. Koch, Phys. Rev. A **77**, 063412 (2008).
[20] D. Reich, M. Ndong, and C. P. Koch, J. Chem. Phys. **136**, 104103 (2012).
[21] L. Greenman, P. J. Ho, S. Pabst, E. Kamarchik, D. A. Mazziotti, and R. Santra, Phys. Rev. A **82**, 023406 (2010).
[22] S. Pabst, L. Greenman, and R. Santra, XCID *Program Package for Multichannel Ionization Dynamics*, Rev. 629, with contributions from P. J. Ho, DESY, Hamburg, Germany, 2011 (unpublished).
[23] D. J. Haxton, K. V. Lawler, and C. W. McCurdy, Phys. Rev. A **83**, 063416 (2011).
[24] D. J. Haxton, K. V. Lawler, and C. W. McCurdy, Phys. Rev. A **86**, 013406 (2012).
[25] O. E. Alon, A. I. Streltsov, and L. S. Cederbaum, J. Chem. Phys. **127**, 154103 (2007).
[26] J. Caillat, J. Zanghellini, M. Kitzler, O. Koch, W. Kreuzer, and A. Scrinzi, Phys. Rev. A **71**, 012712 (2005).
[27] T. Kato and H. Kono, Chem. Phys. **366**, 46 (2009).
[28] M. Nest, R. Padmanaban, and P. Saalfrank, J. Chem. Phys. **126**, 214106 (2007).
[29] I. S. Ulusoy and M. Nest, J. Chem. Phys. **136**, 054112 (2012).
[30] R. P. Miranda, A. J. Fisher, L. Stella, and A. P. Horsfield, J. Chem. Phys. **134**, 244101 (2011).
[31] H. Miyagi and L. B. Madsen, Phys. Rev. A **87**, 062511 (2013).
[32] T. Sato and K. L. Ishikawa, Phys. Rev. A **88**, 023402 (2013).
[33] J. P. Cryan, M. R. Ware, and D. J. Haxton, arXiv:1609.04175.
[34] X. Li, C. W. McCurdy, and D. J. Haxton, Phys. Rev. A **89**, 031404 (2014).
[35] D. J. Haxton and C. W. McCurdy, Phys. Rev. A **90**, 053426 (2014).
[36] K. Bergmann, H. Theuer, and B. W. Shore, Rev. Mod. Phys. **70**, 1003 (1998).
[37] http://www.elettra.trieste.it/FERMI (unpublished).
[38] M. Nest, F. Remacle, and R. D. Levine, New J. Phys. **10**, 025019 (2008).
[39] D. J. Haxton and C. W. McCurdy, Phys. Rev. A **91**, 012509 (2015).
[40] A. Goldberg and B. W. Shore, J. Phys. B **11**, 3339 (1978).
[41] R. Santra and L. S. Cederbaum, Phys. Rep. **368**, 1 (2002).
[42] B. Simon, Phys. Lett. A **71**, 211 (1979).
[43] C. W. McCurdy, M. Baertschy, and T. N. Rescigno, J. Phys. B **37**, R137 (2004).